HHS Public Access

Author manuscript

Nat Chem Biol. Author manuscript; available in PMC 2017 November 08.

Published in final edited form as:

Nat Chem Biol. 2017 July ; 13(7): 730–736. doi:10.1038/nchembio.2376.

Plasticity, dynamics, and inhibition of emerging tetracycline-resistance enzymes

Jooyoung Park[1,*], **Andrew J. Gasparrini**[2,*], **Margaret R. Reck**[3], **Chanez T. Symister**[3], **Jennifer L. Elliott**[1], **Joseph P. Vogel**[1], **Timothy A. Wencewicz**[3,†], **Gautam Dantas**[1,2,4,5,†], and **Niraj H. Tolia**[1,6,†]

[1]Department of Molecular Microbiology, Washington University School of Medicine, St. Louis, Missouri 63110, USA

[2]Center for Genome Sciences & Systems Biology, Washington University School of Medicine, St. Louis, Missouri 63110, USA

[3]Department of Chemistry, Washington University in St Louis, St. Louis, Missouri 63130, USA

[4]Department of Pathology and Immunology, Washington University School of Medicine, St. Louis, Missouri 63110, USA

[5]Department of Biomedical Engineering, Washington University in St. Louis, St. Louis, Missouri 63130, USA

[6]Department of Biochemistry and Molecular Biophysics, Washington University School of Medicine, St. Louis, Missouri 63110, USA

Abstract

While tetracyclines are an important class of antibiotics in agriculture and the clinic, their efficacy is threatened by increasing resistance. Resistance to tetracyclines can occur through efflux, ribosomal protection, or enzymatic inactivation. Surprisingly, tetracycline enzymatic inactivation has remained largely unexplored despite providing the distinct advantage of antibiotic clearance. The tetracycline destructases are a recently-discovered family of tetracycline-inactivating flavoenzymes from pathogens and soil metagenomes with a high potential for broad dissemination. Here, we show tetracycline destructases accommodate tetracycline-class antibiotics

Correspondence and requests for materials should be addressed to N.H.T. (tolia@wustl.edu), G.D. (dantas@wustl.edu), and T.A.W. (wencewicz@wustl.edu).

*These authors contributed equally to this work

†These authors jointly supervised this work (TAW: wencewicz@wustl.edu; GD: dantas@wustl.edu; NHT: tolia@wustl.edu)

Competing Financial Interests: The authors declare no competing financial interests.

Accession codes: The atomic coordinates and structure factors for Tet(50), Tet(51), Tet(55), Tet(50)+chlortetracycline, Tet(50)+anhydrotetracycline, and Tet(56) have been deposited in the RCSB Protein Data Bank under accession codes: 5TUE, 5TUK, 5TUL, 5TUI, 5TUF, and 5TUM respectively.

Author contributions: J.P., designed and performed crystallographic experiments and X-ray structure determination, analyzed data, and wrote the paper; A.J.G., designed and performed *in vitro* and microbiological experiments, analyzed data, and wrote the paper; M.R.R., and C.T.S., performed *in vitro* experiments; J.L.E., performed crystallographic experiments; J.P.V., performed *Legionella* experiments; T.A.W., G.D., and N.H.T., designed experiments, analyzed data, and wrote the manuscript.

in diverse and novel orientations for catalysis, and antibiotic binding drives unprecedented structural dynamics facilitating tetracycline inactivation. We identify a key inhibitor binding mode that locks the flavin adenine dinucleotide cofactor in an inactive state, functionally rescuing tetracycline activity. Our results reveal the potential of a novel tetracycline/tetracycline destructase inhibitor combination therapy strategy to overcome resistance by enzymatic inactivation and restore the use of an important class of antibiotics.

Introduction

Antibiotics revolutionized the treatment of infectious diseases, enabling significant reductions in deaths due to infection over the past 80 years. However, the prolific anthropogenic use of these life-saving chemotherapeutics in the clinic and agriculture has also selected for a steady increase in antibiotic resistance in both benign and pathogenic bacteria[1]. Regrettably, increasing antibiotic resistance has been accompanied by a decrease in development and regulatory approval of new antibiotics[2], threatening the end of the modern antibiotic era. The likely origin of virtually all clinical antibiotic resistance genes are environmental microbial communities, which harbor ancient and diverse resistomes[3-9]. Indeed, environmental reservoirs have been identified for a number of recently-emerged and rapidly-disseminating resistance genes representing urgent clinical threats (e.g. plasmid-borne and chromosomally-acquired carbapenem[10], colistin[11], and quinolone[12] resistance genes). This motivates the need to better understand resistance mechanisms of environmental origin before they are widespread in the clinic and ultimately guide new drug discovery and therapeutic strategies that mitigate emerging mechanisms of resistance.

Despite growing resistance, the tetracyclines remain among the most widely used antibiotics in clinical and agricultural settings[13]. Indeed, tetracyclines ranked in the top three antibiotics in both clinical prescriptions in the United States in 2010 (representing 15% of all antibiotic prescriptions) and in global sales for animal use in 2009 ($500 million in sales)[14]. Furthermore, next-generation derivatives are currently fueling a tetracycline renaissance, with the 2005 clinical approval of tigecycline[15] and ongoing late-stage clinical trials of eravacycline and omadacycline[16,17] justifying urgent interrogation of emerging and novel tetracycline resistance mechanisms. Previously, tetracycline resistance was thought to occur almost exclusively by two mechanisms: ribosomal protection or antibiotic efflux[13,18]. However, an alternate mechanism – enzymatic inactivation – has been documented in benign and pathogenic bacteria, such as the enzyme Tet(X)[19-27]. We recently identified a new family of tetracycline-inactivating enzymes through functional metagenomic selections for tetracycline resistance from 18 grassland and agricultural soils[9]. We showed that these nine proteins, Tet(47-55), were able to enzymatically inactivate tetracycline, resulting in 16-64 fold increases in minimum inhibitory concentration (MIC)[28] when expressed in *E. coli*.

Here, we pursued a multi-pronged structural, *in vitro* enzymatic, and bacterial phenotypic investigation of the emerging tetracycline destructases. We show that a recently identified tetracycline destructase confers tetracycline resistance to a known soil-derived human pathogen. We hypothesized that structural characteristics of tetracycline-inactivating enzymes would reveal useful information about their unique activity profiles and lead to the

rational design of inhibitors, similar to the widely employed β-lactamase inhibitors[29]. Discerning the structural and mechanistic details of conformational or transitional states in target proteins has been crucial for the rational design of successful inhibitors in a number of cases, as exemplified by inhibitors of HIV-1 protease[30] and mechanistic inhibitors of glycosyltransferases that involve significant conformational movement in the active site[31]. Through structure-function analyses of four tetracycline destructases alone and in complex with tetracycline-class ligands, we present the molecular basis for unexpected structural dynamics in tetracycline destructases driven by antibiotic binding. These unprecedented changes provide a novel mechanism for inhibition that has the potential to synergistically restore tetracycline activity and rescue an important class of antibiotics.

Results

Tetracycline inactivation by *Legionella longbeachae*

The tetracycline destructase family was initially discovered by functional metagenomic selection for tetracycline resistance from soil samples[9]. We observed that the soil-derived human pathogen *Legionella longbeachae*, the causative agent of Pontiac Fever and Legionnaires' Disease[32,33] encodes a homolog to the tetracycline destructases, termed *tet*(56). Like the other tetracycline destructases, Tet(56) is able to inactivate tetracycline *in vitro* and expression of *tet*(56) in *E. coli* confers high-level tetracycline resistance[28]. To confirm that *tet*(56) is a functional resistance determinant in *L. longbeachae*, we deleted the gene and examined the strain for changes in drug sensitivity. Deletion of the chromosomally-encoded *tet*(56) resulted in an increase in tetracycline sensitivity to *L. longbeachae* (Fig. 1). Moreover, overexpression of *tet*(56) in the *L. longbeachae* Δ *tet*(56) strain resulted in increased tetracycline resistance to levels even higher than the wild type *L. longbeachae* strain containing vector. Finally, expression of *tet*(56) in *L. pneumophila,* a *Legionella* strain lacking a tetracycline destructase homolog, also dramatically increased the level of tetracycline resistance of the strain. These results demonstrate that tetracycline destructases are already functional in a known human pathogen and their introduction into a related pathogen would lead to increased antibiotic resistance.

Structural architecture and dynamics of Tet(50,51,55,56)

We began our structural analysis by solving the X-ray crystal structures of four tetracycline-inactivating enzymes: Tet(50), Tet(51), Tet(55), and Tet(56) (Fig. 2a and Supplementary Results, Supplementary Fig. 1a-e). Although only sharing ~24% amino acid identity with the previously crystallized Tet(X) and requiring initial structure determination via experimental phasing (Supplementary Table 1), Tet(50,51,55,56) and Tet(X) exhibit a similar overall architecture. Each possesses a flavin adenine dinucleotide (FAD)-binding Rossmann-type fold domain, a tetracycline-binding domain, and a C-terminal α-helix that bridges the two domains (Fig. 2a). Surprisingly, each of the new structures revealed an unexpected second α-helix at the C-terminus (Fig. 2a-c) that is not present in Tet(X) (Fig. 2d) and could not be predicted based on their primary sequences. Comparisons to co-crystal structures of Tet(X) in complex with either chlortetracycline [PDB 2Y6R] or iodtetracycline [PDB 2Y6Q][27] reveal that this helical extension comes in close proximity to the tetracycline binding site (Fig. 2d), contributing to the formation of a substrate-loading channel. In the

Tet(50) crystal structure, we observed two distinct monomers in the asymmetric unit. In Tet(50) monomer A, this substrate-loading channel is blocked by a flexible loop (Fig. 2b,e), whereas in Tet(50) monomer B, the channel is open, allowing tetracycline to access the substrate-binding site (Fig. 2c,f). The absence of the second α-helix in Tet(X) results in a widely exposed entrance to the substrate-binding site (Fig. 2d,g), which likely contributes to alternate substrate specificity of this enzyme.

FAD conformation modulates substrate loading channel

Tetracycline destructases are flavoenzymes that utilize an FAD cofactor to degrade their substrate[34,35]. These enzymes bind FAD in two distinct conformations that are important for catalysis[36]. Both conformations are captured by the structures presented here (Supplementary Fig. 1f-j). Tet(50) monomer A, which has a closed substrate-loading channel, bound FAD in an IN conformation (Fig. 2h). In this conformation the reactive isoalloxazine moiety of the FAD is stretched away from the adenosine moiety and into the substrate-binding site. This allows reaction with molecular oxygen to produce an FAD-hydroperoxide intermediate that is in close proximity to the tetracycline substrate (the C4a of FAD is ~5.9 Å away from the C11a substrate hydroxylation site in Tet(X)), allowing for hydroxylation and subsequent spontaneous degradation of the tetracycline substrate[37]. After catalysis, FAD flips away from the substrate-binding site, adopting the OUT conformation. Tet(50) monomer B, which has an open substrate-loading channel, binds FAD in an OUT conformation where the isoalloxazine moiety is bent towards the adenosine and away from the substrate-binding site (Fig. 2i). This conformational change allows for products to be released through the open channel and positions the oxidized FAD for reduction by NADPH in a distinct NADPH binding site during cofactor regeneration (Fig. 2j and Fig. 3a)[37]. After reduction, FAD is poised to flip back to the IN conformation for the next round of catalysis upon substrate binding. Our observation of FAD in both IN and OUT conformations implies that FAD exists in an equilibrium between the two states in the absence of substrate binding.

Substrate binding drives FAD and channel conversion

Since accessibility of the substrate-loading channel appeared to be dependent on the conformation of FAD in the Tet(50) crystal structures, we soaked Tet(50) with various tetracycline compounds. Surprisingly, chlortetracycline binds to Tet(50) in a ~180° rotated orientation compared to the orientation in which chlortetracycline and other tetracycline substrates (*e.g.* iodtetracycline, minocycline, tigecycline) bind Tet(X)[27,38] (Fig. 3a-d and Supplementary Fig. 2). Tetracycline compounds have a four-ring system (labeled A-D (Figure 3a,c), and have a distinctive three-dimensional architecture with a significant bend between rings A and B, allowing for unambiguous modeling into the electron density. In the Tet(X)+chlortetracycline structure, the chlortetracycline D-ring with the attached chlorine faces away from the substrate-binding site and towards bulk solvent (Fig. 3c,d). This places the C11a substrate hydroxylation site of ring C proximal to FAD. In the Tet(50)+chlortetracycline structure, the D-ring chlorine now faces FAD with the dimethylamine group of the A-ring making van der Waals contacts with Phe-95 from the flexible loop, Val-348 from the first C-terminal α-helix, and Ile-371 from the second C-terminal α-helix (Fig. 3a,b). Surprisingly, this new orientation positions C11a of chlortetracycline away from C4a of FAD.

We observed a second notable characteristic when comparing the structures of Tet(50) in the presence or absence of chlortetracycline. In the absence of chlortetracycline, Tet(50) monomer A had FAD in an IN conformation with a closed channel (Fig. 2e,f,k,l) and monomer B had FAD in an OUT conformation with an open channel (Fig. 2g,h,m,n). However, in the presence of chlortetracycline, we only detected bound chlortetracycline in monomer B, which now had FAD in an IN conformation and a closed channel (Fig. 3e-h). Thus, substrate binding to Tet(50) monomer B induced a conformational switch from FAD OUT to FAD IN and loop closure (Fig. 3h,i).

Tetracycline destructases degrade chlortetracycline

Due to the unanticipated orientation of chlortetracycline binding, we examined whether the tetracycline destructases could degrade chlortetracycline. Enzymatic reactions were analyzed at several time points by reverse-phase high-performance liquid chromatography (HPLC). We observed the time- and enzyme-dependent degradation of chlortetracycline by Tet(50) and Tet(X) (Fig. 4a). Kinetic parameters of enzymatic inactivation were determined by monitoring *in vitro* reaction progress using absorbance at 400 nm. The catalytic efficiency of Tet(50) was five times higher than that of Tet(X) (k_{cat}/K_M values of 0.55 and $0.11 \mu M^{-1} min^{-1}$, respectively) (Supplementary Table 2). This increased efficiency is primarily due to increased turnover as the apparent K_M values are comparable between Tet(50) (6.3±2.0 μM) and Tet(X) (7.9±2.7 μM) in spite of different substrate binding orientations. Tet(55) and Tet(56) also degraded chlortetracycline *in vitro* with 4-fold and 15-fold greater efficiency than Tet(X), respectively (Supplementary Table 2). Furthermore, *tet*(50,51,55,56,X) each confer chlortetracycline resistance when expressed in *E. coli* at levels 16–32 fold greater than the vector-only control (Supplementary Table 3). As a result, despite employing a distinct mode of substrate binding, Tet(50,51,55,56) are able to degrade chlortetracycline more efficiently than Tet(X).

Tetracycline inactivation by Tet(X) occurs via catalysis at C11a resulting in a product of *m/z* 461[28]. Because chlortetracycline binds Tet(50) in an alternative mode that positions C11a far away from the reactive flavin peroxide moiety, we sought to characterize the degradation product to establish substrate hydroxylation. Enzymatic reactions were analyzed by liquid chromatography-mass spectrometry (Supplementary Fig. 3), and found to convert chlortetracycline (*m/z* 479) to an oxidation product with an *m/z* of 467. This is in contrast to the *m/z* 461 monooxygenation product observed for tetracycline[28], consistent with an alternate binding mode for chlortetracycline. To further characterize this product, reactions were subjected to high resolution mass spectrometry (Fig. 4b). Reactions with each enzyme assayed (Tet(50,55,56)) yielded a primary product with an exact *m/z* of 467.12 (Supplementary Fig. 4a-d).

In the alternative binding mode, the nonplanarity of the chlortetracycline substrate positions the reactive A-ring C3 in closest proximity to the flavin cofactor. Notably, the C3 is 6.1Å (Fig. 4c) and the C1 carbonyl is 7.4 Å (Fig. 4d) from the C4a of the flavin cofactor. These distances are similar to C11a of chlortetracycline and C4a of FAD in the Tet(X) +chlortetracycline structure[27], and well within the C4a-reactive atom distances observed for flavin monooxygenases[39]. The C11a in the Tet(50)+chlortetracycline, on the other hand, is

on the opposite side of the molecule and 7.9 Å away (Fig. 4e). Accordingly, we propose a mechanism in which the flavin peroxide attacks C3 of the chlortetracycline A ring, yielding intermediate **1** (Supplementary Fig. 4e). Spontaneous epoxide formation gives intermediates **2** and **3**, which rearranges to a cycloheptanone intermediate **5** via Baeyer-Villiger ring expansion. Expulsion of carbon monoxide yields intermediate **6**, and ring contraction yields oxidation product **7**, with an *m/z* of 467. Alternatively, intermediate **3** can be formed by flavin peroxide attack of C1 of the chlortetracycline A ring, via intermediate **4**, and then similarly continuing through products **5-7**. The final product **7** is consistent with the fragmentation pattern observed in tandem mass spectrometry (Fig. 4b). Similar oxidative cascades proceeding through Baeyer-Villiger reactions have been observed in the biosynthesis of the cyclic type II polyketide mithramycin by the flavin monooxygenase MtmOIV[40]. The discovery of alternative substrate binding modes and characterization of degradation products demonstrates the plasticity of tetracycline destructases for adapting flavoenzyme-mediated degradation chemistries to achieve resistance in the presence of diverse tetracycline scaffolds.

Anhydrotetracycline locks the FAD in an OUT conformation

Due to the global dissemination of the β-lactamases, nearly all β-lactam antibiotics are co-developed with β-lactamase inhibitors[29], an approach that has successfully prolonged their clinical utility. We reasoned that a similar strategy might be useful to counteract tetracycline resistance by inactivation, and therefore sought to identify small molecule inhibitors of these enzymes. Previously, we observed that anhydrotetracycline, a key biosynthetic precursor[41] and degradation product[42] of tetracycline with poor antibiotic activity was not degraded by Tet(47-56)[28]. None the less, it is known to be an effector of tetracycline producers and tetracycline-resistant bacteria by inducing expression of energetically expensive tetracycline efflux pumps, permitting tetracycline producers to survive and selecting against tetracycline resistance[43]. Based on the structural similarity to tetracycline and the intimate role that anhydrotetracycline plays in tetracycline biology, we hypothesized that anhydrotetracycline represents an evolutionarily-privileged chemical lead for inhibitor design.

We obtained a co-crystal structure of Tet(50) with anhydrotetracycline bound, and observed two unique features in comparison to our Tet(50)+chlortetracycline and the earlier Tet(X) +chlortetracycline structures. First, anhydrotetracycline binds to Tet(50) in a flipped orientation and in a position distinct from where chlortetracycline binds (Fig. 5a-c and Supplementary Fig. 5-6). The unique binding mode for anhydrotetracycline is enabled by the lack of a 6-hydroxyl group of ring C present in tetracycline or chlortetracycline (Fig. 5a). Without this substitution at the 6 position, the tetracycline gains additional aromatic stabilization. The resultant planar structure allows the 6-methyl group to make van der Waals interactions with a conserved Thr/Ser at residue position 207 in Tet(47-56) (Fig. 5d and Supplementary Fig. 6-7). Thr-207 would cause a steric clash with the 6-methyl and 6-hydroxyl groups of ring C in tetracycline or chlortetracycline, explaining the distinct binding modes.

The second interesting feature is that when anhydrotetracycline was bound, FAD was in the OUT conformation and the substrate-loading channel was open (Fig. 5b,c). The unique

binding location of anhydrotetracycline locks the isoalloxazine moiety of FAD away from the substrate-binding site and sterically blocks the transition to the FAD IN conformation observed in the Tet(50)+chlortetracycline monomer B. This unexpected binding mode establishes a novel mechanism for inhibitors that stabilize the inactive OUT conformation of the FAD cofactor in flavoenzymes and prevents transition to the necessary FAD IN conformation for catalysis. Therefore, anhydrotetracycline is a mechanistic inhibitor of the tetracycline destructases that also competitively blocks substrate binding.

Anhydrotetracycline inhibits tetracycline destructases

We examined the effect of anhydrotetracycline on tetracycline destructase activity *in vitro*. We performed *in vitro* enzymatic reactions in the presence or absence of anhydrotetracycline followed by HPLC. For clinical relevance, we first focused on Tet(56), the tetracycline destructase from pathogenic *L. longbeachae*. We observed the Tet(56)-dependent degradation of 0.1 mM tetracycline over time, as demonstrated by the decrease in the tetracycline peak (Fig. 6a). However, in the presence of 1 mM anhydrotetracycline, the tetracycline peak does not change, indicating that tetracycline is not degraded (Fig. 6b). Similar results were observed for Tet(50,51,55,X) (Supplementary Fig. 8, Supplementary Table 4). We also monitored enzymatic inactivation of tetracycline using absorbance at 400 nm in the presence of a range of anhydrotetracycline concentrations. Anhydrotetracycline inhibited Tet(50,55,56) with IC_{50} values of 83.2±1.2μM, 25.6±1.2μM, and 37.1±1.1μM, respectively (Fig. 6c). Thus, anhydrotetracycline prevents the enzyme-dependent degradation of tetracycline. Together with our structural data, this indicates a common mechanism of inhibition for tetracycline-inactivating enzymes, and establishes anhydrotetracycline as a lead compound that presents a flexible starting point for generating tetracycline destructase inhibitors with improved activity[44]. This inhibition strategy that stabilizes inactive cofactor states is widely applicable to the larger superfamily of flavoenzymes and offers new avenues for inhibiting any member of this superfamily, many of which have been implicated in human disease and represent promising targets for hypercholesterolemia and antifungal drugs[45].

Novel inhibition mechanism restores tetracycline activity

Our data suggest that a tetracycline/tetracycline-destructase-inhibitor (e.g. anhydrotetracycline) combination therapy strategy could potentially be employed to rescue antibiotic activity of tetracyclines against bacteria that encode tetracycline-inactivating enzymes. Tet(X) and Tet(56) are of particular interest due to their clinical significance. *tet*(X) has been recently identified in a number of human pathogens, including 11 nosocomial uropathogens from Sierra Leone[46] and 12 *Acinetobacter baumannii* isolates from a hospital in China[47]. We also showed that *tet*(56) is present and functional in *L. longbeachae*[28] – a pathogen responsible for causing Pontiac Fever and Legionnaires' Disease[32,33]. Accordingly, we tested whether anhydrotetracycline rescues tetracycline efficacy against *E. coli* expressing *tet*(56). Two μg/mL anhydrotetracycline caused a greater than 5-fold change in sensitivity of *E. coli* expressing *tet*(56) to tetracycline in liquid culture, as indicated by a change in IC_{50} from 47.4 to 8.27 μg/mL (Fig. 6d). Further, anhydrotetracycline and tetracycline acted synergistically to inhibit growth of *E. coli* expressing Tet(50,51,55,56), with fractional inhibitory concentration indices (FICI) of 0.625,

0.5, 0.375 and 0.1875, respectively (Fig. 6e and Supplementary Fig. 9). Although anhydrotetracycline is not degraded by Tet(47-56), it is slowly degraded by Tet(X)[28]. However, anhydrotetracycline still was able to prevent tetracycline degradation by Tet(X) *in vitro* (Supplementary Fig. 8). Our proof of concept experiment, taken together with our structural and *in vitro* data, reveals that a co-administration strategy based on inhibition of tetracycline-inactivating enzymes could be effective for the treatment of tetracycline-resistant bacterial infections.

Discussion

The widespread anthropogenic use of tetracycline antibiotics motivates the immediate study of emerging mechanisms of tetracycline resistance, such as enzymatic inactivation. Our data provide unprecedented insight into the dynamics of tetracycline-inactivating enzymes and reveal a novel mode of inhibition. Substrates like chlortetracycline are loaded into enzymes in the FAD OUT conformation through the substrate-loading channel (Supplementary Fig. 10a), which is open as a flexible loop is pulled away from the channel. Upon substrate binding, the enzyme converts to FAD IN, the channel closes, and catalysis can occur due to the proximity of FAD to the substrate. Mechanistic inhibitors like anhydrotetracycline also enter the enzyme through the same channel but bind at a distinct site (Supplementary Fig. 10b). Binding of inhibitor in this location sterically blocks FAD conversion to the IN conformation and prevents subsequent substrate binding and catalysis. Our model predicts that compounds that either bind with higher affinity to the inhibitor binding pocket, or that concomitantly bind to the inhibitor and substrate-binding sites will provide enhanced inhibition for the control of tetracycline resistance. This novel mechanism of inhibition is not only applicable to preventing antibiotic resistance, but is highly relevant to additional FAD dependent enzymes that comprise the flavoenzyme superfamily and are of clinical interest[45].

The rise in resistance to early-generation tetracyclines has spurred the development of next-generation derivatives, including tigecycline (approved for human use in 2005)[15], and eravacycline and omadacycline (currently in late-stage clinical trials)[16,17]. These newer drugs are designed to evade resistance by efflux or ribosomal protection, but they are largely untested against tetracycline-inactivating enzymes. Alarmingly, tigecycline was found to be vulnerable to oxidative inactivation by Tet(X)[27], which was recently identified for the first time in numerous pathogens of high clinical concern[46,47]. These challenges highlight the immediate importance of studying mechanisms of emerging tetracycline resistance, such as those described here that expand substrate scope.

Tetracycline resistance by enzymatic inactivation has thus far been rarely documented compared to resistance by efflux or ribosomal protection. Growing evidence, however, indicates that enzymatic tetracycline inactivation is a widespread feature in soil microbial communities[28], and is a recently observed emerging threat in human pathogens[46-48]. Flavoenzymes display a proclivity for horizontal gene transfer and gene duplication, bestowing the potential to spread between bacteria and acquire novel functions[49]. Interestingly, the contigs on which *tet*(47-55) were discovered also contained mobility elements and other resistance genes[9,28],suggesting that their original genomic context may

be as part of a multidrug resistance cassette or mobile genetic element. This indicates that tetracycline-inactivating enzymes pose a threat for facile acquisition by additional human pathogens. Indeed, we show that *tet*(56) is present and functional in the human pathogen *L. longbeachae*, and *tet*(X) has now been reported in four out of six ESKAPE pathogens[46-48], demonstrating the urgency of this threat. Our results reveal the structural basis for plasticity and dynamics in substrate binding in these enzymes. We propose a novel combination therapy strategy to retain tetracycline efficacy against bacteria that harbor tetracycline-inactivating resistance genes. Our results provide the structural and biochemical foundation to counter the alarming emergence of tetracycline resistance via enzymatic inactivation.

Online Methods

Legionella plasmid construction

The Tet(56) deletion plasmid, pJB7204, was constructed by amplifying 2 kb of DNA upstream and downstream of the Tet(56) ORF using primers JVP2913/JVP2910 and JVP2911/JVP2912 and *Legionella longbeachae* chromosomal DNA. The PCR products were digested with SalI/NotI and NotI/SacI, respectively, and ligated into SalI/SacI-digested suicide vector pSR47S[50]. The ligated product was transformed into EC100D::Δpir and selected on LB plates containing 20 μg/ml kanamycin. The Tet(56) complementing clone, pJB7207, was constructed by amplifying the Tet(56) ORF using primers JVP2921/JVP2922 and *Legionella longbeachae* chromosomal DNA. The PCR product was digested with BamHI/SalI and cloned into BamHI/SalI-digested expression vector pJB1625 (Supplementary Table 5).

Legionella strain construction

The Tet(56) deletion strain, JV8858, was constructed by a traditional loop-in/loop-out strategy. Briefly, the wild type *Legionella longbeachae* strain JV595 was transformed by electroporation with the ΔTet(56) suicide plasmid pJB7204 and integrants were selected on CYE plates[51] containing 30 μg/ml kanamycin. Resolution of the merodiploid was obtained on CYE plates containing sucrose. Strains were then electroporated with the vector pJB1625 or the Tet(56) complementing clone pJB7207 and transformants were selected on CYE plates containing 5 μg/ml chloramphenicol.

Tetracycline inactivation in *Legionella*

Antibiotic susceptibility testing was performed using *L. longbeachae* wild type and deletion strains and *L. pneumophila*[52], bearing either the vector pJB1625[53] or the Tet(56) complementing clone pJB7207. Minimum inhibitory concentrations were determined according to Clinical and Laboratory Standards Institute (CLSI) procedures with the following modifications. Results are representative of three independent experiments. The strains were initially grown as a patch on CYE plates containing chloramphenicol for 2 days at 37 degrees. The bacteria were swabbed into distilled water, washed one time, and resuspended at an 600 nm absorbance (OD_{600}) of 1 (~1E9 CFU/ml). The culture was diluted 200 fold into 10 mL of buffered AYE media containing 2 μg/ml chloramphenicol and a range of tetracycline but lacking supplemental iron, as iron can interfere with tetracycline

activity. The cultures were grown for 48 hours at 37°C on a roller drum and the absorbances (OD_{600}) were periodically measured using a Genesys 20 Spectrophotometer.

Cloning, expression and purification of tetracycline-inactivating enzymes

All genes encoding tetracycline-inactivating enzymes were cloned into the pET28b(+) vector (Novagen) at BamHI and NdeI restriction sites. Constructs were transformed into BL21-Star (DE3) competent cells (Life Technologies). Cells harboring the plasmid were grown at 37°C in LB medium containing a final concentration of 0.03 mg/mL kanamycin. Once cells reached an OD_{600} of 0.6, cells were cooled to 15 °C and induced with 1 mM IPTG overnight. After this period, cells were harvested by centrifugation at 4000 rpm for 10 min at 4 °C. Cell pellets were suspended in 10 mL of 50 mM Tris (pH 8.0), 100 mM NaCl, 10 mM imidazole (pH 8.0), 1 mM PMSF, and 5 mM BME per 1 liter of LB medium and stored at −80°C.

Cells were thawed in the presence of 0.25 mg/mL lysozyme and disrupted using sonication on ice for 60 seconds. The cell extract was obtained by centrifugation at 13,000 rpm for 30 min at 4 °C and was applied onto nickel rapid run agarose beads (Goldbio) equilibrated with wash buffer (50 mM Tris (pH 8.0), 150 mM NaCl, 20 mM imidazole (pH 8.0), and 5 mM BME). The wash buffer was used to wash the nickel column three times with five column volumes. After washing, protein was eluted with five column volumes of elution buffer (wash buffer with 300 mM imidazole). The protein sample was further purified by gel chromatography using a HiLoad 16/600 Superdex 200pg column (GE Healthcare) equilibrated with 10 mM Tris (pH 8.0), 150 mM NaCl, 5 mM dithioerythritol (DTT). The fractions containing the protein of interest were pooled and concentrated using a 30K MWCO Amicon centrifugal filter (Millipore).

Tet(55) selenomethionine-labelling

For selenomethionine-labelled Tet(55) (Se-Met Tet(55)), cells were grown in 1 L of SelenoMet™ Medium supplemented with SelenoMet Nutrient Mix (Molecular Dimensions Limited). Once cells reached an OD_{600} of 0.6, feedback inhibition amino acid mix (0.1 g of lysine, threonine, phenylalanine; 0.05 g of leucine, isoleucine, valine; 0.05 g of L(+) selenomethionine (ACROS Organics 259960025)) was added and the cells were shaken for 15 minutes at 15 °C. After 15 minutes, cells were induced at 15 °C with 1 mM IPTG overnight. All other purification conditions were the same as for the native tetracycline-inactivating enzymes.

Crystallization, data collection, and structure determination

For crystallization, Se-Met Tet(55) was concentrated to 25 mg/mL. Crystals were obtained by vapor diffusion using hanging drops equilibrated at 18 °C. Se-Met Tet(55) crystallized in 0.1 M Tris-HCl (8.5) and 20–25% PEG 3000. Se-Met Tet(55) crystals were harvested directly from the growth condition and flash-frozen under liquid nitrogen.

Native Tet(55) was concentrated to 50 mg/mL and crystallized in 0.1 M Tris-HCl (8.5) and 25–27% PEG 4000. Native Tet(55) crystals were harvested directly from the growth condition and flash-frozen. Tet(50) was concentrated to 35 mg/mL and crystallized in 0.1 M

MES (pH 6.0–6.5), 1.6–2.0 M ammonium sulfate, 2–10% 1,4-Dioxane. Crystals were harvested directly from the growth condition and flash-frozen. For co-crystal structures, Tet(50) was concentrated to 17 mg/mL, and Tet(50) crystals were soaked with mother liquor plus 5 mM chlortetracycline or 4 mM anhydrotetracycline for 30 minutes before flash-freezing. Tet(51) was concentrated to 13 mg/mL and crystallized in 0.1 M MES (pH 6.0) and 10% PEG 6000. Crystals were cryo-protected with 0.1 M MES (pH 6.0), 10% PEG 6000, and 30% glycerol before flash-freezing. Tet(56) was concentrated to 38 mg/mL and crystallized in 0.1 M tri-sodium citrate (pH 5.6), 10% PEG 4000, 10% isopropanol. Tet(56) crystals were cryo-protected in 0.1 M tri-sodium citrate (pH 5.6), 10% PEG 4000, 10% isopropanol, and 20% glycerol before flash-freezing.

The crystal structure of Tet(55) was solved by seleno-methionine labeling and single-wavelength anomalous dispersion (SAD) (Supplementary Table 1), as molecular replacement using the previously published Tet(X) structures was unsuccessful. The inability to solve the structure by molecular replacement demonstrates that tetracycline-inactivating enzymes are structurally diverse and multiple structures are required to capture the diversity within the family. X-ray data for selenomethionine-labelled Tet(55) were collected from a single crystal using a wavelength of 0.976289 Å at synchrotron beamline 4.2.2 of the Advanced Light Source in Berkeley, CA. All other native data sets were collected at a wavelength of 1 Å. Data were collected on the CMOS detector and were processed with XDS[54]. Structure solution for Se-Met Tet(55) was performed using PHENIX AutoSol. Thirteen selenium sites were found, which gave a figure of merit of 0.370. The resulting Tet(55) model was refined against the native Tet(55) data set. R and R_{free} flags were imported from the Se-Met Tet(55) mtz file using UNIQUEIFY within the CCP4 package[55]. Tet(50,51,56) structures were solved my PHENIX AutoMR using an ensemble of three domains of Tet(55) (domain 1 = aa1–70, aa100–172, aa276–319; domain 2= aa71–99, 173–275; domain 3= aa320–387). Structure solution for the Tet(50) chlortetracycline and anhydrotetracycline structures were performed by refinement with the apo Tet(50) structure, from which the R and R_{free} flags were imported using UNIQUEIFY.

Subsequent iterated manual building/rebuilding and refinement of models were performed using Coot[56] and PHENIX[57], respectively. The structure validation server MolProbity[58] was used to monitor refinement of the models. All final refined models have favorable crystallographic refinement statistics, as provided in Supplementary Table 1. Figures were generated and rendered in PyMOL Molecular Graphics System, Version 0.99rc6, Schrödinger, LLC.

In vitro tetracycline and chlortetracycline inactivation assays

Reactions were prepared in 100 mM TAPS buffer with 100 μM substrate, 14.4 μM enzyme, and an NADPH regenerating system consisting of the following components (final concentrations): glucose-6-phosphate (40 mM), $NADP^+$ (4 mM), $MgCl_2$ (1 mM), and glucose-6-phosphate dehydrogenase (4U/ml). The regeneration system was incubated at 37°C for 30 minutes to generate NADPH before use in reactions. Reactions were sampled at various timepoints, and quenched in four volumes of an acidic quencher consisting of equal parts acetonitrile and 0.25 M HCl.

Products generated from enzymatic inactivation of both tetracycline and chlortetracycline were separated by reverse phase HPLC using a Phenomenex Luna C18 column (5μm, 110 Å, 2×50 mm) and 0.1% trifluoroacetic acid in water (A) and acetonitrile (B) as mobile phase. Injections of 25μl sample volume were eluted using a linear gradient from 25%B to 75%B over 14 minutes at a flow rate of 1 ml/min.

Chlortetracycline reactions analyzed by high resolution tandem mass spectrometry were sampled at 75 minutes. The quenched samples were diluted 6× with 50% methanol in 0.1% formic acid and run on the Q-Exactive Orbitrap by direct infusion using the Advion Triversa nanomate. The data were acquired with resolution of 140,000. The MS scan was acquired from m/z 300 – 550. MS/MS spectra were acquired on the m/z 467.12 compounds.

Tetracycline inactivation in *E. coli*

Antibiotic susceptibility testing was performed in *E. coli* MegaX cells (Invitrogen) bearing the pZE21 expression vector with the tetracycline inactivating gene of interest. Minimum inhibitory concentrations were determined according to Clinical and Laboratory Standards Institute (CLSI) procedures[59] using Mueller-Hinton broth with 50 μg/mL kanamycin and a range of chlortetracycline concentrations profiled via absorbance measurements at 600 nm (OD_{600}) at 45 minute intervals using the Synergy H1 microplate reader (Biotek Instruments, Inc) for 48 hours at 37°C.

Kinetic characterization of tetracycline and chlortetracycline inactivation

The optimal enzyme concentration for steady-state kinetics assays was determined by varying the concentration of enzyme while keeping chlortetracycline and NADPH concentration constant. 0.4 μM enzyme was found to give linear slopes for all concentrations of substrate tested, and was used as the enzyme concentration for all kinetics experiments.

Reactions were prepared in 100 mM TAPS buffer at pH 8.5 with 0–160 μM substrate, 1.6 mM NADPH, and 0.4 μM enzyme. UV-visible spectroscopy measurements were taken in triplicate at 400 nm wavelength light with a Cary 60 UV/Vis system (Agilent) for 10 minutes at room temperature. Initial reaction velocities were determined by linear regression using the Agilent Cary WinUV Software, and fitted to the Michaelis-Menten equation:

$$v_0 = \frac{V_{\max}[S]}{K_M + [S]}$$

using GraphPad Prism 6.

LC-MS characterization of chlortetracycline degradation products

Reactions were prepared in 100 mM phosphates buffer at pH 8.5 with 1 mM CTC, 0.5 mM NADPH, 5 mM MgCl2 and 0.4 μM Tet(55). After 10 minutes, the reaction was centrifuge filtered for 10 minutes using a Millipore Amicon Ultracel (3 kDa MW cutoff) to remove enzyme. Prior to centrifugation, filters were triply rinsed with phosphate buffer to remove excess glycerol. The filtrate was collected and analyzed by LC-MS using an Agilent 6130

single quadrupole instrument with G1313 autosampler, G1315 diode array detector, and 1200 series solvent module. Reaction products were separated using a Phenomenex Gemini C18 column, 50 × 2 mm (5 μm) with guard column cassette was used with a linear gradient of 0% acetonitrile + 0.1% formic acid to 95% acetonitrile + 0.1% formic acid over 14 min at a flow rate of 0.5 mL/min prior to analysis by electrospray ionization.

In vitro characterization of anhydrotetracycline inhibition

IC_{50} values were determined for Tet(50), Tet(55), and Tet(56) by measuring the initial velocity of tetracycline degradation in the presence of varying concentrations of anhydrotetracycline. The concentrations of tetracycline and NADPH were kept constant at 25 μM and 500 μM, respectively. Assays were prepared by combining all components except for enzyme and equilibrating to 25°C for five minutes. After the addition of enzyme, absorbance at 400 nm was measured for five minutes. All measurements were taken in triplicate. The final concentrations for assay components were 100 mM TAPS buffer (pH 8.5), 25 μM tetracycline, 500 μM NADPH, 16 mM $MgCl_2$, 0.4 μM enzyme, and 0.05 – 150 μM anhydrotetracycline. A control assay using no anhydrotetracycline was assigned a concentration of 1.0×10^{-15} μM for analysis. A second control using no enzyme and 100 μM anhydrotetracycline was assigned a concentration of 1.0×10^{15} μM to simulate full inhibition of enzyme. IC_{50} values were determined by plotting the log of anhydrotetracycline concentration against v_0 in GraphPad Prism 6. Functional Tet(51) expressed poorly, so Tet(51) was omitted from these and other in vitro experiments.

Checkerboard synergy assay

Tetracycline (1024 μg/mL) and anhydrotetracycline (256 μg/mL) were dissolved in cation-adjusted Mueller-Hinton broth supplemented with 50 ug/mL kanamycin. A twofold dilution series of each drug was made independently across 8 rows of a 96 well master plate before 100 uL of each drug dilution series were combined into a 96 well culture plate (Costar), with rows included for no-drug and no-inocula controls. A sterile 96-pin replicator (Scinomix) was used to inoculate plates with ~1 uL of *E. coli* MegaX (Invitrogen) expressing a tetracycline inactivating enzyme, diluted to OD_{600} 0.1 using. Plates were sealed with Breathe-Easy membranes (Sigma-Aldrich) and incubated at 37°C with shaking at 220 rpm. Endpoint growth was determined by OD_{600} at 20 and 36 hours of growth using a Synergy H1 plate reader (BioTek, Inc.). Three independent replicates were performed for each strain on separate days. Synergy of anhydrotetracycline and tetracycline combinations was determined using the fractional inhibitory concentration index (FICI) method[60],

$$\mathrm{FICI}=\frac{\mathrm{MIC}A_{\mathrm{combo}}}{\mathrm{MIC}A_{\mathrm{alone}}}+\frac{\mathrm{MIC}B_{\mathrm{combo}}}{\mathrm{MIC}B_{\mathrm{alone}}}$$

where FICI>1 indicates antagonism, FICI = 1 indicates additivity, and FICI <1 indicates synergy. The efficacy of the drug combination was also evaluated in the *L. longbeacheae* background, but synergy was not observed.

Data Availability

The atomic coordinates and structure factors for Tet(50), Tet(51), Tet(55), Tet(50)+chlortetracycline, Tet(50)+anhydrotetracycline, and Tet(56) have been deposited in the RCSB Protein Data Bank under accession codes: 5TUE, 5TUK, 5TUL, 5TUI, 5TUF, and 5TUM respectively. All other data generated or analyzed during this study are included in this published article (and its Supplementary Information files) or are available from the corresponding author on reasonable request.

Supplementary Material

Refer to Web version on PubMed Central for supplementary material.

Acknowledgments

We thank J. Nix and ALS beamline 4.2.2 (contract DE-AC02-05CH11231) for assistance with X-ray data collection and A. Durairaj of the Proteomics & Mass Spectrometry Facility at the Danforth Plant Science Center for assistance with HR-MS/MS experiments. This work was supported by an award to N.H.T, G.D., and T.A.W. from the National Institute of Allergy and Infectious Diseases of the National Institutes of Health (R01 AI123394). A.J.G. is supported by the National Institute of General Medical Sciences Cell and Molecular Biology Training Grant (T32 GM007067). The content is solely the responsibility of the authors and does not necessarily represent the official views of the funding agencies.

References

1. Knapp CW, Dolfing J, Ehlert PA, Graham DW. Evidence of increasing antibiotic resistance gene abundances in archived soils since 1940. Environ Sci Technol. 2010; 44:580–587. DOI: 10.1021/es901221x [PubMed: 20025282]
2. Kinch MS, Patridge E, Plummer M, Hoyer D. An analysis of FDA-approved drugs for infectious disease: antibacterial agents. Drug Discov Today. 2014; 19:1283–1287. DOI: 10.1016/j.drudis.2014.07.005 [PubMed: 25043770]
3. Davies J. Inactivation of antibiotics and the dissemination of resistance genes. Science. 1994; 264:375–382. [PubMed: 8153624]
4. Allen HK, et al. Call of the wild: antibiotic resistance genes in natural environments. Nat Rev Microbiol. 2010; 8:251–259. DOI: 10.1038/nrmicro2312 [PubMed: 20190823]
5. Berendonk TU, et al. Tackling antibiotic resistance: the environmental framework. Nat Rev Microbiol. 2015; 13:310–317. DOI: 10.1038/nrmicro3439 [PubMed: 25817583]
6. Benveniste R, Davies J. Aminoglycoside Antibiotic-Inactivating Enzymes in Actinomycetes Similar to Those Present in Clinical Isolates of Antibiotic-Resistant Bacteria. Proc Natl Acad Sci U S A. 1973; 70:2276–2280. [PubMed: 4209515]
7. D'Costa VM, et al. Antibiotic resistance is ancient. Nature. 2011; 477:457–461. DOI: 10.1038/nature10388 [PubMed: 21881561]
8. Forsberg KJ, et al. The shared antibiotic resistome of soil bacteria and human pathogens. Science. 2012; 337:1107–1111. DOI: 10.1126/science.1220761 [PubMed: 22936781]
9. Forsberg KJ, et al. Bacterial phylogeny structures soil resistomes across habitats. Nature. 2014; 509:612–616. DOI: 10.1038/nature13377 [PubMed: 24847883]
10. Yong D, et al. Characterization of a new metallo-beta-lactamase gene, bla(NDM-1), and a novel erythromycin esterase gene carried on a unique genetic structure in Klebsiella pneumoniae sequence type 14 from India. Antimicrob Agents Chemother. 2009; 53:5046–5054. DOI: 10.1128/aac.00774-09 [PubMed: 19770275]
11. Liu YY, et al. Emergence of plasmid-mediated colistin resistance mechanism MCR-1 in animals and human beings in China: a microbiological and molecular biological study. Lancet Infect Dis. 2016; 16:161–168. DOI: 10.1016/s1473-3099(15)00424-7 [PubMed: 26603172]

12. Poirel L, Rodriguez-Martinez JM, Mammeri H, Liard A, Nordmann P. Origin of plasmid-mediated quinolone resistance determinant QnrA. Antimicrob Agents Chemother. 2005; 49:3523–3525. DOI: 10.1128/aac.49.8.3523-3525.2005 [PubMed: 16048974]
13. Thaker M, Spanogiannopoulos P, Wright GD. The tetracycline resistome. Cell Mol Life Sci. 2010; 67:419–431. DOI: 10.1007/s00018-009-0172-6 [PubMed: 19862477]
14. State of the World's Antibiotics, 2015. Center for Disease Dynamics, Economics & Policy; Washington, D.C.: 2015.
15. Kasbekar N. Tigecycline: a new glycylcycline antimicrobial agent. Am J Health Syst Pharm. 2006; 63:1235–1243. DOI: 10.2146/ajhp050487 [PubMed: 16790575]
16. Sutcliffe JA, O'Brien W, Fyfe C, Grossman TH. Antibacterial activity of eravacycline (TP-434), a novel fluorocycline, against hospital and community pathogens. Antimicrob Agents Chemother. 2013; 57:5548–5558. DOI: 10.1128/AAC.01288-13 [PubMed: 23979750]
17. Macone AB, et al. In vitro and in vivo antibacterial activities of omadacycline, a novel aminomethylcycline. Antimicrob Agents Chemother. 2014; 58:1127–1135. DOI: 10.1128/aac.01242-13 [PubMed: 24295985]
18. Chopra I, Roberts M. Tetracycline antibiotics: mode of action, applications, molecular biology, and epidemiology of bacterial resistance. Microbiol Mol Biol Rev. 2001; 65:232–260. second page, table of contents. DOI: 10.1128/mmbr.65.2.232-260.2001 [PubMed: 11381101]
19. Park BH, Levy SB. The cryptic tetracycline resistance determinant on Tn4400 mediates tetracycline degradation as well as tetracycline efflux. Antimicrob Agents Chemother. 1988; 32:1797–1800. [PubMed: 3072922]
20. Speer BS, Salyers AA. Characterization of a novel tetracycline resistance that functions only in aerobically grown Escherichia coli. J Bacteriol. 1988; 170:1423–1429. [PubMed: 2832361]
21. Whittle G, Hund BD, Shoemaker NB, Salyers AA. Characterization of the 13-kilobase ermF region of the Bacteroides conjugative transposon CTnDOT. Appl Environ Microbiol. 2001; 67:3488–3495. DOI: 10.1128/aem.67.8.3488-3495.2001 [PubMed: 11472924]
22. Nonaka L, Suzuki S. New Mg2+-dependent oxytetracycline resistance determinant tet 34 in Vibrio isolates from marine fish intestinal contents. Antimicrob Agents Chemother. 2002; 46:1550–1552. [PubMed: 11959596]
23. Diaz-Torres ML, et al. Novel tetracycline resistance determinant from the oral metagenome. Antimicrob Agents Chemother. 2003; 47:1430–1432. [PubMed: 12654685]
24. Ghosh S, Sadowsky MJ, Roberts MC, Gralnick JA, LaPara TM. Sphingobacterium sp. strain PM2-P1-29 harbours a functional tet(X) gene encoding for the degradation of tetracycline. J Appl Microbiol. 2009; 106:1336–1342. DOI: 10.1111/j.1365-2672.2008.04101.x [PubMed: 19187139]
25. Yang W, et al. TetX is a flavin-dependent monooxygenase conferring resistance to tetracycline antibiotics. J Biol Chem. 2004; 279:52346–52352. DOI: 10.1074/jbc.M409573200 [PubMed: 15452119]
26. Moore IF, Hughes DW, Wright GD. Tigecycline is modified by the flavin-dependent monooxygenase TetX. Biochemistry. 2005; 44:11829–11835. DOI: 10.1021/bi0506066 [PubMed: 16128584]
27. Volkers G, Palm GJ, Weiss MS, Wright GD, Hinrichs W. Structural basis for a new tetracycline resistance mechanism relying on the TetX monooxygenase. FEBS Lett. 2011; 585:1061–1066. DOI: 10.1016/j.febslet.2011.03.012 [PubMed: 21402075]
28. Forsberg KJ, Patel S, Wencewicz TA, Dantas G. The tetracycline destructases: a novel family of tetracycline inactivating enzymes. Chemistry and Biology. 2015; 22:888–897. [PubMed: 26097034]
29. Drawz SM, Papp-Wallace KM, Bonomo RA. New beta-lactamase inhibitors: a therapeutic renaissance in an MDR world. Antimicrob Agents Chemother. 2014; 58:1835–1846. DOI: 10.1128/aac.00826-13 [PubMed: 24379206]
30. Hornak V, Okur A, Rizzo RC, Simmerling C. HIV-1 protease flaps spontaneously close to the correct structure in simulations following manual placement of an inhibitor into the open state. J Am Chem Soc. 2006; 128:2812–2813. DOI: 10.1021/ja058211x [PubMed: 16506755]

31. Pesnot T, Jorgensen R, Palcic MM, Wagner GK. Structural and mechanistic basis for a new mode of glycosyltransferase inhibition. Nat Chem Biol. 2010; 6:321–323. DOI: 10.1038/nchembio.343 [PubMed: 20364127]
32. Cazalet C, et al. Analysis of the Legionella longbeachae genome and transcriptome uncovers unique strategies to cause Legionnaires' disease. PLoS Genet. 2010; 6:e1000851. [PubMed: 20174605]
33. Whiley H, Bentham R. Legionella longbeachae and legionellosis. Emerg Infect Dis. 2011; 17:579–583. DOI: 10.3201/eid1704.100446 [PubMed: 21470444]
34. Ballou DP, Entsch B, Cole LJ. Dynamics involved in catalysis by single-component and two-component flavin-dependent aromatic hydroxylases. Biochem Biophys Res Commun. 2005; 338:590–598. DOI: 10.1016/j.bbrc.2005.09.081 [PubMed: 16236251]
35. van Berkel WJ, Kamerbeek NM, Fraaije MW. Flavoprotein monooxygenases, a diverse class of oxidative biocatalysts. J Biotechnol. 2006; 124:670–689. DOI: 10.1016/j.jbiotec.2006.03.044 [PubMed: 16712999]
36. Gatti DL, et al. The mobile flavin of 4-OH benzoate hydroxylase. Science. 1994; 266:110–114. [PubMed: 7939628]
37. Massey V. Activation of molecular oxygen by flavins and flavoproteins. J Biol Chem. 1994; 269:22459–22462. [PubMed: 8077188]
38. Volkers G, et al. Putative dioxygen-binding sites and recognition of tigecycline and minocycline in the tetracycline-degrading monooxygenase TetX. Acta Crystallogr D Biol Crystallogr. 2013; 69:1758–1767. DOI: 10.1107/s0907444913013802 [PubMed: 23999299]
39. Liu LK, et al. The Structure of the Antibiotic Deactivating, N-hydroxylating Rifampicin Monooxygenase. J Biol Chem. 2016; 291:21553–21562. DOI: 10.1074/jbc.M116.745315 [PubMed: 27557658]
40. Gibson M, Nur-e-alam M, Lipata F, Oliveira MA, Rohr J. Characterization of kinetics and products of the Baeyer-Villiger oxygenase MtmOIV, the key enzyme of the biosynthetic pathway toward the natural product anticancer drug mithramycin from Streptomyces argillaceus. J Am Chem Soc. 2005; 127:17594–17595. DOI: 10.1021/ja055750t [PubMed: 16351075]
41. Wang P, Bashiri G, Gao X, Sawaya MR, Tang Y. Uncovering the enzymes that catalyze the final steps in oxytetracycline biosynthesis. J Am Chem Soc. 2013; 135:7138–7141. DOI: 10.1021/ja403516u [PubMed: 23621493]
42. Yuen PH, Sokoloski TD. Kinetics of concomitant degradation of tetracycline to epitetracycline, anhydrotetracycline, and epianhydrotetracycline in acid phosphate solution. J Pharm Sci. 1977; 66:1648–1650. [PubMed: 21284]
43. Palmer AC, Angelino E, Kishony R. Chemical decay of an antibiotic inverts selection for resistance. Nat Chem Biol. 2010; 6:105–107. DOI: 10.1038/nchembio.289 [PubMed: 20081825]
44. Liu F, Myers AG. Development of a platform for the discovery and practical synthesis of new tetracycline antibiotics. Curr Opin Chem Biol. 2016; 32:48–57. DOI: 10.1016/j.cbpa.2016.03.011 [PubMed: 27043373]
45. Lienhart WD, Gudipati V, Macheroux P. The human flavoproteome. Arch Biochem Biophys. 2013; 535:150–162. DOI: 10.1016/j.abb.2013.02.015 [PubMed: 23500531]
46. Leski TA, et al. Multidrug-resistant tet(X)-containing hospital isolates in Sierra Leone. Int J Antimicrob Agents. 2013; 42:83–86. DOI: 10.1016/j.ijantimicag.2013.04.014 [PubMed: 23688520]
47. Deng M, et al. Molecular epidemiology and mechanisms of tigecycline resistance in clinical isolates of Acinetobacter baumannii from a Chinese university hospital. Antimicrob Agents Chemother. 2014; 58:297–303. DOI: 10.1128/aac.01727-13 [PubMed: 24165187]
48. Boucher HW, et al. Bad bugs, no drugs: no ESKAPE! An update from the Infectious Diseases Society of America. Clin Infect Dis. 2009; 48:1–12. DOI: 10.1086/595011 [PubMed: 19035777]
49. Walsh CT, Wencewicz TA. Flavoenzymes: versatile catalysts in biosynthetic pathways. Nat Prod Rep. 2013; 30:175–200. DOI: 10.1039/c2np20069d [PubMed: 23051833]

online Methods References

50. Merriam JJ, Mathur R, Maxfield-Boumil R, Isberg RR. Analysis of the Legionella pneumophila fliI gene: intracellular growth of a defined mutant defective for flagellum biosynthesis. Infect Immun. 1997; 65:2497–2501. [PubMed: 9169800]
51. Feeley JC, et al. Charcoal-yeast extract agar: primary isolation medium for Legionella pneumophila. J Clin Microbiol. 1979; 10:437–441. [PubMed: 393713]
52. Berger KH, Isberg RR. Two distinct defects in intracellular growth complemented by a single genetic locus in Legionella pneumophila. Mol Microbiol. 1993; 7:7–19. [PubMed: 8382332]
53. Sexton JA, et al. The Legionella pneumophila PilT homologue DotB exhibits ATPase activity that is critical for intracellular growth. J Bacteriol. 2004; 186:1658–1666. [PubMed: 14996796]
54. Kabsch W. XDS. Acta Crystallogr D Biol Crystallogr. 2010; 66:125–132. DOI: 10.1107/s0907444909047337 [PubMed: 20124692]
55. Winn MD, et al. Overview of the CCP4 suite and current developments. Acta Crystallogr D Biol Crystallogr. 2011; 67:235–242. DOI: 10.1107/s0907444910045749 [PubMed: 21460441]
56. Emsley P, Cowtan K. Coot: model-building tools for molecular graphics. Acta Crystallogr D Biol Crystallogr. 2004; 60:2126–2132. DOI: 10.1107/s0907444904019158 [PubMed: 15572765]
57. Adams PD, et al. PHENIX: a comprehensive Python-based system for macromolecular structure solution. Acta Crystallogr D Biol Crystallogr. 2010; 66:213–221. DOI: 10.1107/s0907444909052925 [PubMed: 20124702]
58. Chen VB, et al. MolProbity: all-atom structure validation for macromolecular crystallography. Acta Crystallogr D Biol Crystallogr. 2010; 66:12–21. DOI: 10.1107/s0907444909042073 [PubMed: 20057044]
59. Methods for Dilution Antimicrobial Susceptibility Testing for Bacteria That Grow Aerobically; Approved Standard--Tenth Edition. Vol. M07-A10. Clinical and Laboratory Standards Institute; 2015. CLSI.
60. Berenbaum MC. A method for testing for synergy with any number of agents. J Infect Dis. 1978; 137:122–130. [PubMed: 627734]

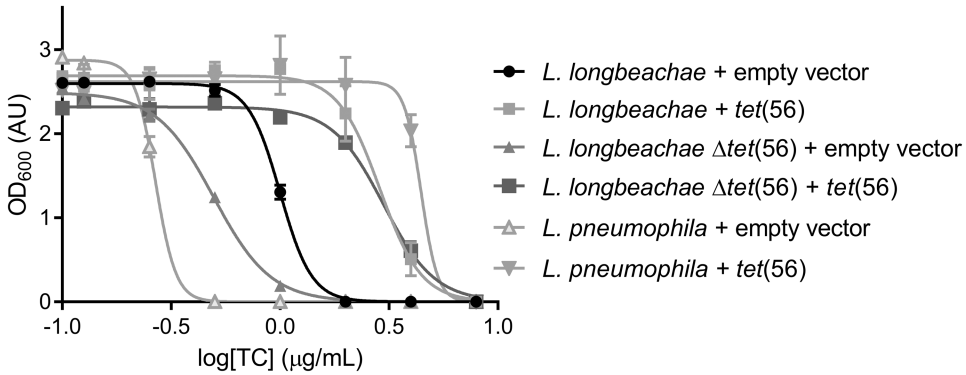

Figure 1. Dose-response curve showing the effect of tetracycline on growth of *Legionella* strains

Deletion of *tet*(56) from *L. longbeachae* causes an increase in tetracycline sensitivity. Complementation with a plasmid containing the *tet*(56) insert rescues the tetracycline resistance phenotype compared to strains bearing the empty-vector control. Furthermore, introduction of the complementing vector into *L. pneumophila*, which lacks a *tet*(56) homolog, results in an increase in tetracycline resistance. Data are represented as mean ± s.d. of three technical replicates.

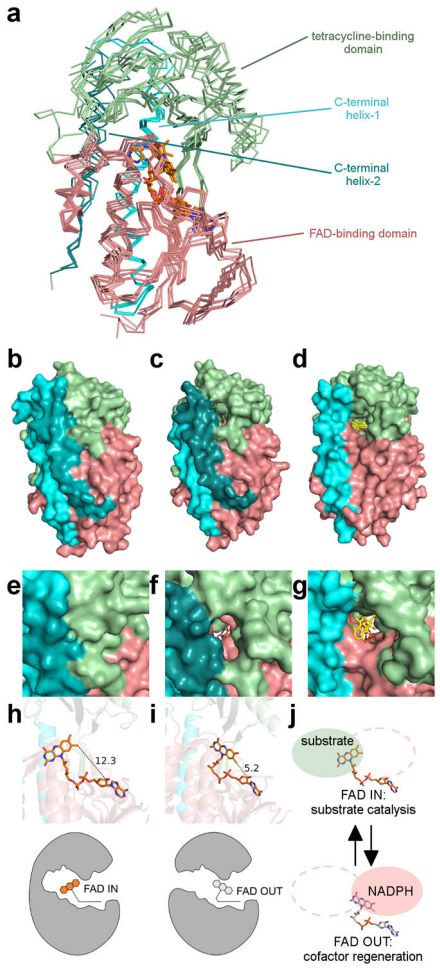

Figure 2. Crystal structures of Tet(50), Tet(51), Tet(55), and Tet(56) reveal a conserved architecture, structural changes that enable substrate loading channel accessibility, and two conformations of the FAD cofactor

(a) Overlay of the Tet(50) monomer A, Tet(50) monomer B, Tet(51), Tet(55), and Tet(56) crystal structures. The FAD-binding domain (salmon), the tetracycline-binding domain (pale green), the first (cyan) and second (deep teal) C-terminal α-helixes, and FAD molecules (orange) are shown. **b-d** Surface representation of **(b)** Tet(50) monomer A with the substrate-loading channel closed, **(c)** Tet(50) monomer B with the substrate-loading channel open, and **(d)** a previously published structure of Tet(X) with chlortetracycline (yellow) bound – PDB ID 2Y6R. **e-g** Zoomed in view of **(e)** the closed substrate-loading channel in Tet(50) monomer A **(f)** the open substrate-loading channel in Tet(50) monomer B, and **(g)** the wide open substrate-binding site in Tet(X). **(h)** The FAD cofactor adopts the IN conformation in Tet(50) monomer A, characterized by a 12.3 Å distance between the C8M and C2B atoms of the FAD molecule **(i)** The FAD cofactor adopts the OUT conformation in Tet(50) monomer B, characterized by a 5.2 Å distance between the C8M and C2B atoms of the FAD molecule. **(j)** The IN conformation of FAD allows for substrate catalysis. The OUT conformation of FAD allows for regeneration of the reduced FAD for the next round of catalysis. The green area indicates the substrate-binding site. The pink area indicates the putative NADPH binding site.

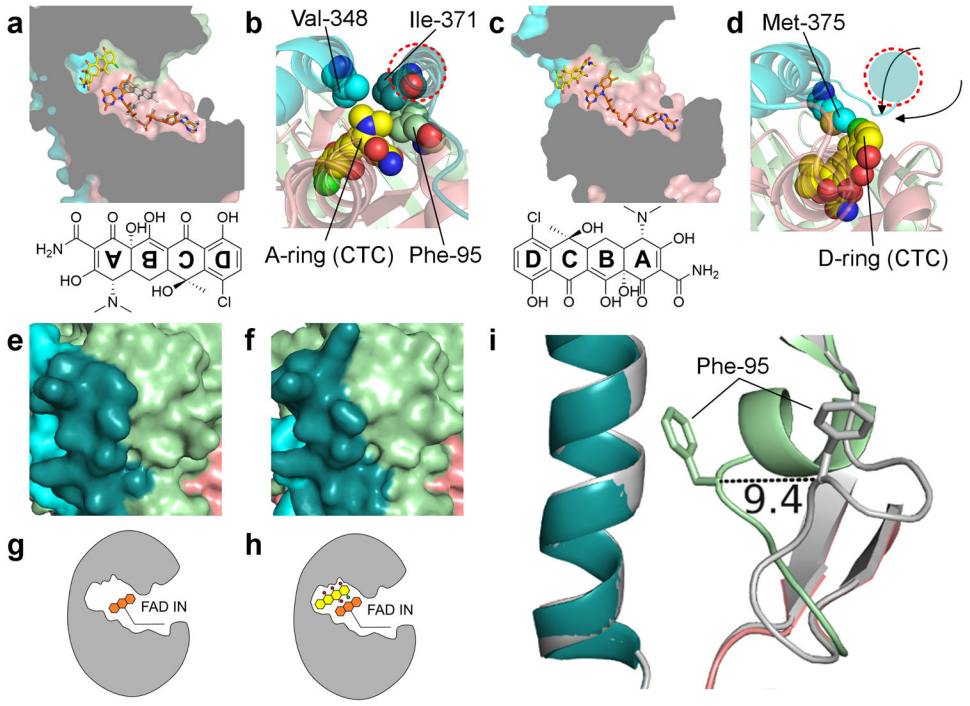

Figure 3. Tet(50)+chlortetracycline structure reveals an unexpected mode of binding that drives substrate loading channel closure and FAD conversion

(a) Chlortetracycline binds to Tet(50) in a ~180° rotated orientation relative to Tet(X) +chlortetracycline, with FAD IN (orange); a model of FAD OUT (grey) is overlaid. **(b)** The rotated orientation in the Tet(50)+chlortetracycline structure is supported by van der Waals contacts from Val-348 (cyan) and Ile371 (deep teal) of the two C-terminal α-helices in Tet(50) to the dimethylamine group of the A-ring of chlortetracycline. Additionally, Phe-95 from the flexible loop makes contacts with the dimethylamine group and closes off the substrate-binding site. **(c)** Chlortetracycline binds Tet(X) with the D-ring distal to FAD. The substrate-binding site is widely exposed to bulk solvent. **(d)** Met-375 from the first C-terminal α-helix in Tet(X) (cyan) makes van der Waals contacts to the D-ring of chlortetracycline. A second C-terminal helix (red dashed circle, colored in deep teal) does not exist in Tet(X), and substrate can potentially enter from various possible directions. **(e)** Surface representation of Tet(50)+chlortetracycline monomer A. **(f)** Surface representation of Tet(50)+chlortetracycline monomer B. **(g)** In Tet(50)+chlortetracycline monomer A, FAD is IN, the loop is closed, and no chlortetracycline is bound. **(h)** In Tet(50)+chlortetracycline monomer B, FAD is IN, the loop is closed, and chlortetracycline is bound. **(i)** While the substrate-loading channel is open in Tet(50) monomer B, with FAD OUT, in the absence of chlortetracycline (grey), the flexible loop containing Phe-95 closes over the channel in Tet(50)+chlortetracycline monomer B, with FAD now IN.

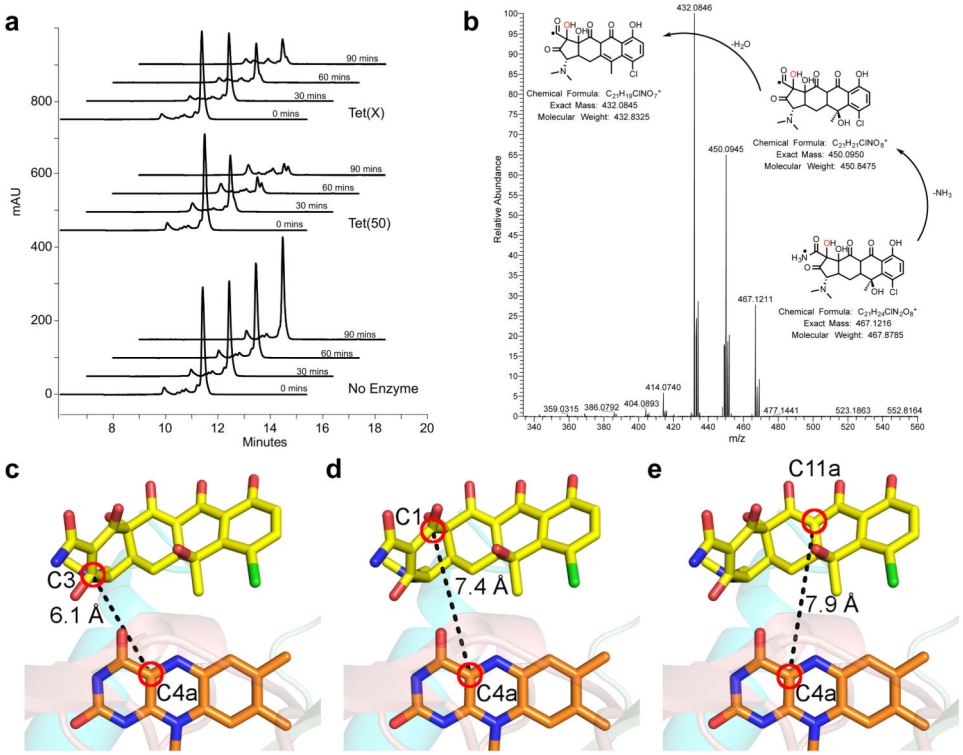

Figure 4. Chlortetracycline is degraded by tetracycline destructases despite the unusual binding mode

(a) HPLC chromatograms show the time and enzyme dependent consumption of chlortetracycline. **(b)** High-resolution MS-MS analysis of the tetracycline destructase reaction with chlortetracycline supports clean conversion to the m/z 467 oxidation product. MS-MS spectrum of the m/z 467 ion from the Tet(55) reaction with proposed fragmentation pathway. **c-e** The closest reactive carbons to C4a of the FAD cofactor are C3 **(c)** and C1 **(d)** of the chlortetracycline A ring, both of which are closer than C11a **(e)**, the hydroxylation site observed in Tet(X) mediated chlortetracycline degradation.

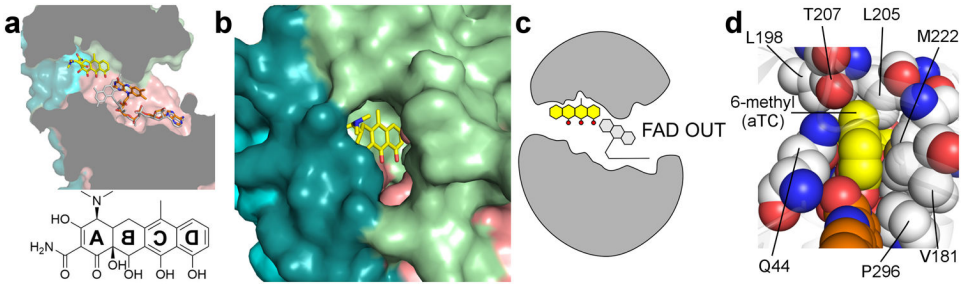

Figure 5. Anhydrotetracycline binds to the active site of Tet(50), trapping FAD in the unproductive OUT conformation

(a) Anhydrotetracycline binds the active site of Tet(50) and traps the FAD cofactor in the unproductive OUT conformation (orange) in monomer B. The IN conformation of FAD from monomer A is superimposed in grey for comparison, and sterically clashes with the D-ring hydroxyl of anhydrotetracycline. **(b)** Surface representation of Tet(50)+anhydrotetracycline reveals that the substrate-loading channel remains open, which corresponds to FAD locked in the OUT conformation. **(c)** In Tet(50)+anhydrotetracycline monomer B, FAD is OUT, the loop is open, and anhydrotetracycline is bound (not shown: in monomer A, FAD is IN, the loop is closed, no anhydrotetracycline is bound). **(d)** Residue Thr-207 in Tet(50) makes van der Waals interactions with the planar 6-methyl group of anhydrotetracycline (aTC) (yellow) in the bound orientation, but would sterically clash with the 6-methyl and 6-hydroxyl groups that branch from the C ring of tetracycline or chlortetracycline if bound in a flipped orientation.

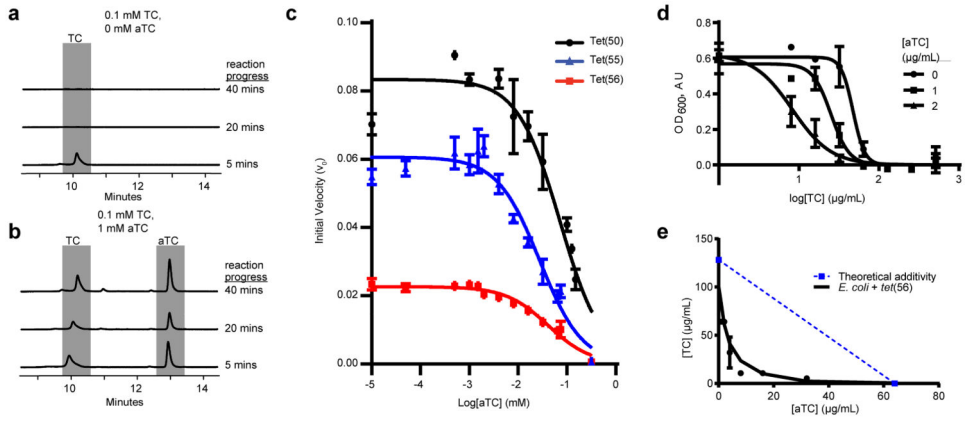

Figure 6. Anhydrotetracycline prevents enzymatic tetracycline degradation, functionally rescuing tetracycline antibiotic activity

(a) Tetracycline (TC) is degraded by Tet(56) *in vitro* HPLC chromatograms show *in vitro* reactions with UV detection at 363 nm and separation on a C18 column. **(b)** TC degradation is attenuated by the addition of an excess of aTC. **(c)** Dose-dependent inhibition of Tet(50,51,56) activity by anhydrotetracycline. Velocity is determined by measuring tetracycline consumption via change in absorbance at 400 nm. Data are represented as mean ± s.d. of three technical replicates. **(d)** Dose-response curve showing effect of aTC on sensitivity of Tet(56)-expressing *E. coli* to TC in liquid culture. Data are represented as mean ± s.e.m. of three technical replicates. **(e)** TC and aTC synergistically inhibit growth of *E. coli* expressing Tet(56), FICI = 0.1875. Points show minimum inhibitory concentrations of two drugs in combination. Dashed line indicates the theoretical concentration of additive drug interaction. Data represented as mean ± s.e.m. of three technical replicates.